X-Ray Diffraction with Molten Au_xMn_{100-x}-Alloys

R. M. Hagenmayer[a], P. Lamparter[b], and S. Steeb[b]

[a] Institute Laue-Langevin, B.P. 156, F-38042 Grenoble Cedex 9
[b] Max-Planck-Institut für Metallforschung, Seestraße 92, D-70174 Stuttgart

Z. Naturforsch. **50a**, 831–836 (1995); received June 1, 1995

The molten alloys $Au_{28.5}Mn_{71.5}$ and $Au_{68}Mn_{32}$ are investigated with the energy dispersive X-ray diffraction method which works rather fast so that the evaporation loss of Mn from the molten alloys is kept low. From the observed prepeak follows that both melts are compound-forming but the gold rich melt $Au_{68}Mn_{32}$ shows only 50% of the short range order existent within the $Au_{28.5}Mn_{71.5}$ melt. Total structure factors and total pair correlation functions are discussed.

1. Introduction

During the investigation of molten alloys with X-ray diffraction one needs a large $Q = 4\pi \frac{\sin\Theta}{\lambda}$ – range (2Θ = Bragg angle, λ = wavelength) and rather short exposure times in order to keep the molten surface clean and to suppress partial evaporation of the molten material. This leads to the combination of a Θ–Θ-diffractometer [1] with the energy dispersive X-ray diffraction (EDXD) method. The EDXD-method was already applied to the study of crystalline [2], molten [3], and amorphous [4, 5] materials.

With the EDXD-method, the primary beam contains the continuous spectrum, and the diffracted radiation is detected by a solid state energy-sensitive detector arranged at a fixed scattering angle 2Θ. The advantage of this method is that structural information is obtained up to a large momentum transfer Q. In real space this results in a high resolution around the first maximum of the atomic distribution function.

Pratt [6] observed for molten $Au_{50}Mn_{50}$ a strong compound forming tendency, whereas with the Au-rich alloys ($c_{Au} \geq 0.7$) the formation of like atomic pairs, i.e. Mn–Mn, dominates. In the present work the molten alloys $Au_{28.5}Mn_{71.5}$ and $Au_{68}Mn_{32}$ are studied (see also [7]).

Reprint requests to Prof. S. Steeb.

2. Theoretical

2.1 Total Structure Factor and Total Pair Correlation Function

The total structure factor $S(Q)$ according to Faber-Ziman [8] follows from the coherently scattered intensity per atom $I_{co}(Q)$:

$$S(Q) = \frac{I_{co}(Q) - [\langle f(Q)^2\rangle - \langle f(Q)\rangle^2]}{\langle f(Q)\rangle^2} \tag{1}$$

with

$f_i(Q)$ = atomic scattering amplitude of component i,

$\langle f(Q)^2\rangle = \sum_{i=1}^{n} c_i f_i^2$, $\langle f(Q)\rangle = \sum_{i=1}^{n} c_i f_i$

c_i = atomic fraction of component i,

n = number of components forming the alloy.

From $S(Q)$ one obtains the total pair correlation function

$$G(R) = \frac{2}{\pi}\int_0^\infty Q\,[S(Q) - 1]\sin(Q\,R)\,\mathrm{d}Q, \tag{2}$$

where R = distance in real space.

$G(R)$ finally yields the pair distribution function

$$g(R) = \frac{G(R)}{4\pi\varrho_0 R} + 1 \tag{3}$$

with ϱ_0 = mean atomic number density.

The number of atoms in a spherical shell with radii between $R_i - \frac{1}{2}\Delta R$ and $R_i + \frac{1}{2}\Delta R$ amounts to

$$N(R_i) = \int_{R_i - \frac{\Delta R}{2}}^{R_i + \frac{\Delta R}{2}} 4\pi R^2 \varrho_0\, g(R)\,\mathrm{d}R. \tag{4}$$

0932-0784 / 95 / 0900-0831 $ 06.00 © – Verlag der Zeitschrift für Naturforschung, D-72027 Tübingen

2.2 EDXD-Method

The intensity $I_{exp}(E, \Theta)$ scattered from the specimen is composed of a coherent and an incoherent contribution:

$$I_{exp}(E,\Theta) = C\epsilon(E) \cdot (I_0(E)P(E,\Theta)A(E,\Theta)[I_{co} + I_{ms,co}]_{E,\theta} + I_0(E')P(E,E',\Theta)A(E,E',\Theta)\cdot[I_{in} + I_{ms,in}]_{E',\theta}) \quad (5)$$

with

C = normalization constant,
$\epsilon(E)$ = detector efficiency,
$I_0(E)$ = intensity of the primary spectrum,
$P(E,\Theta)$ = polarization correction,
$A(E,\Theta)$ = absorption correction,
$I_{co}(E,\Theta)$ = coherent single scattering intensity per atom,
$I_{ms,co}$ = coherent multiple scattering intensity per atom,
$I_{ms,in}$ = incoherent multiple scattering intensity per atom,
$I_{in}(E',\Theta)$ = incoherent single scattering intensity per atom (Compton-scattering),
E' = Energy of the primary X-ray photon which is reduced by the Compton-effect to the energy E:

$$E' = E + \Delta E = \frac{E}{1 - 0.00391\, E \sin^2\Theta}.$$

Concerning a comprehensive discussion of all these terms and their determination during the evaluation procedure we refer to [9].

Finally, the structure factor $S(Q)$ is obtained from (1) and (5) using

$$Q = (4\pi/hc)\, E \sin\Theta, \quad (6)$$
$$= 1.0135\, E \sin\Theta \ ([Q] = \text{Å}^{-1}, [E] = \text{keV}),$$

h = Planck's constant, c = speed of light.

For the EDXD-method one uses the Bremsstrahlung and keeps the scattering angle 2Θ constant. Thus Q-values up to 28 $Å^{-1}$ may be reached, which is to be compared to maximum 16 $Å^{-1}$ with the usual angular dispersive diffraction (ADXD) method if MoK_α radiation is used.

The integrated intensity of the Bremsstrahlung is larger than that of the characteristic radiation. This means shorter exposure times, which is essential during the investigation of molten alloys because of possible variations of the composition caused by partial evaporation. Time dependent errors are excluded by the EDXD-method, since the pulses of all energies are counted at the same time.

The disadvantages of the EDXD-method compared to the ADXD-method are:

i) The energy spectrum has to be determined and
ii) the semiconductor detector has a limited energy resolution of 165 eV at the energy of 5.9 keV. This value was measured by the manufacturer using the ^{52}Fe-isotopic radiation.

During the present work the resolution was determined using the X-radiation from the W-tube which was used during the present investigation, with the results of 300 eV at 20 keV and 340 eV at 40 keV. This resolution is sufficient for the investigation of melts and amorphous substances. For the lattice parameter determination of crystalline materials the accuracy is smaller than with ADXD by a factor of ten.

The counting efficiency of the Si(Li) detector depends on the quantum energy to be detected and can be calculated according to a relationship given in [10]. The calculation yields a decrease of the efficiency from 100% at 20 keV down to 66% at 40 keV.

3. Experimental

3.1 Θ–Θ-EDXD Apparatus

A Θ–Θ diffractometer [1, 11] was supplied with a Si(Li)-detector in order to render possible EDXD. Figure 1 shows the arrangement. The weight of the Si(Li) including liquid nitrogen (altogether 15 kg) was balanced by the weight G_2. The angle between cryostat and detector amounts to 22.5° to achieve a high level of liquid nitrogen within the cryostat during scanning the Θ-angle region between 0° and 45°. A tube with tungsten anode was used because its characteristic lines are outside the energy range of 20 keV up to 40 keV which is relevant for the evaluation. Corresponding to (6) we obtain with $E_{max} = 40$ keV and $\Theta_{max} = 45°$ the value $Q_{max} \approx 28$ $Å^{-1}$.

The useful energy range is limited experimentally by the following facts:

i) The characteristic radiation of the anode material, namely W–L_α, W–L_β, and W–L_γ and the characteristic Au- and Mn-radiations from the molten alloy occur at energies < 20 keV, which therefore must be excluded from the evaluation procedure.
ii) The energies > 40 keV have to be excluded since in that region the detector efficiency decreases

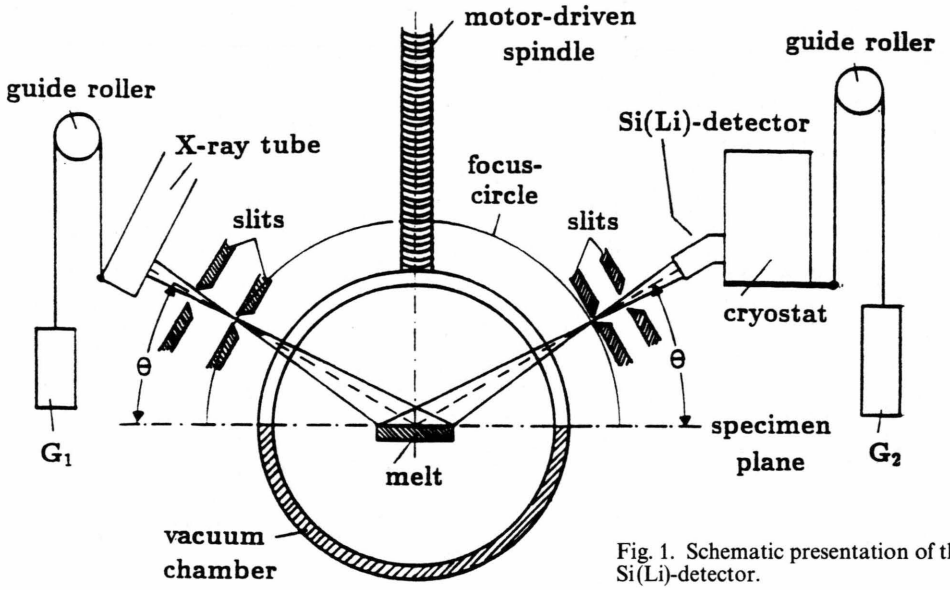

Fig. 1. Schematic presentation of the $\Theta-\Theta$ goniometer with Si(Li)-detector.

strongly and since $W-K_\alpha$ and $W-K_\beta$ radiation occurs. Thus for the Au–Mn-melts an energy window between 20 keV and 40 keV was chosen for data evaluation.

This limitation in the energy range means that for a distinct 2Θ-angle only a limited Q-range can be evaluated according to (6). Thus, for the determination of $S(Q)$ for an extended Q-range measurements at different 2Θ-angles are necessary. Figure 2 shows the choice of six 2Θ-values used for the present measurements.

3.1.1 High Temperature Specimen Chamber

Two molybdenum electrodes supply two graphite sheets, each of the dimensions $70 \times 20 \times 0.8$ mm^3 with heating current. The graphite sheets bear the crucible of boronnitride with a diameter of 50 mm which cotains the melt and whose bottom contains within a hole the W 5%Re–W 25%Re-thermocouple. Perpendicular to the scattering plane the specimen was surrounded by an Al_2O_3-ring coated along the inner circumference with Mo-foil which reflects the radiation heat emitted from the specimen. Because of the rather high partial vapour pressure of Mn within molten Au_xMn_{1-x} at high temperatures the investigation could not be done under vacuum but in a protecting atmosphere of helium 6N at pressures between 5 Torr and 20 Torr. A hot niobium wire was used as getter material.

3.1.2 Computer Control

Figure 3 shows a schematic diagram of the experimental set up. The primary beam is collimated by the slits S_1 and S_2. The diffracted beam reaches the Si(Li)-detector through the slits S_3 and S_4. The detector and the preamplifier (PRAMP) are cooled by liquid nitrogen (LN_2) which is controlled by a monitor (LN_2–M). The intensities measured at a fixed angle are stored by a multichannel analyzer (MCA) as $I(E)$-presentation. For this procedure one needs a spectroscopy amplifier (SP AMP) and an analog-digital converter (ADC). A computer (PC) controls the MCA, the step motor control (SMC), and the furnace control (FC).

3.2 Experimental Procedure

3.2.1 Energy Spectrum of the Bremsstrahlung

To determine the energy spectrum of the primary beam the method of diffraction with a gas was used [12]. The vacuum chamber was filled with Argon, and different runs at low scattering angles were made.

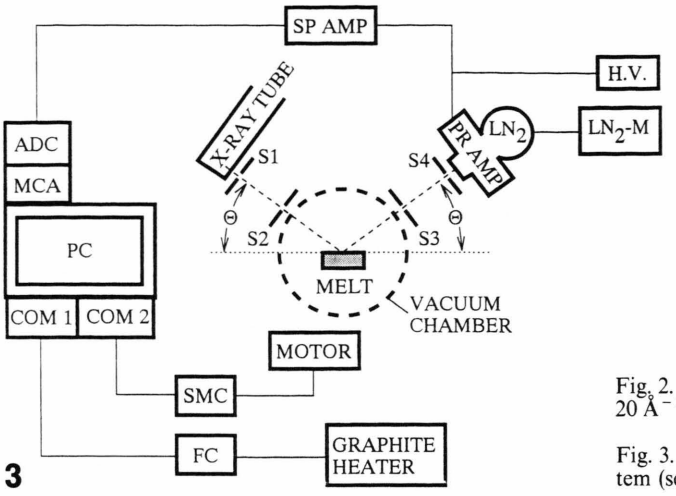

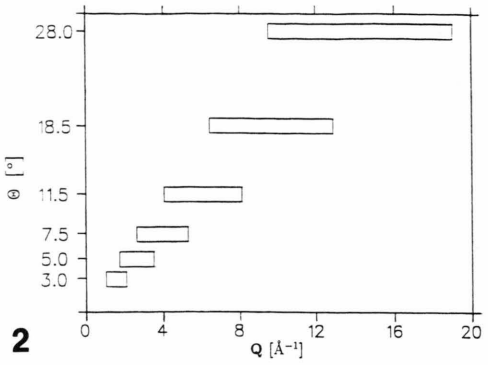

Fig. 2. Choice of Θ-angles to cover the Q-region up to 20 $Å^{-1}$.

Fig. 3. Schematic presentation of the computer control system (see text).

3.2.2 Specimen Preparation

The Au–Mn phase diagram shows two eutectic regions, the first at 28.5% gold (1095 °C) and the second at 68% gold (960 °C). These two alloys were produced using gold (99.99%) and manganese (99.9%). Before melting, the manganese was cleaned using HNO_3 and dried in argon. The alloys were melted within an Al_2O_3-crucible by induction heating and cast into a copper mold.

3.2.3 Diffraction Experiments

The specimen was heated for twelve hours in vacuum (10^{-5} Torr) up to 300–350 °C in order to degass all parts of the vacuum chamber. Then the specimen was melted during six to eight hours. The diffraction experiment consisted of two to three runs with one hour each. The alloy $Au_{28.5}Mn_{71.5}$ was investigated at 1145 °C, 15 Torr He, the alloy $Au_{68}Mn_{32}$ at 1010 °C, 10 Torr He. Figure 4 shows as an example the measured intensities from molten $Au_{28.5}Mn_{71.5}$ for a fixed angle of $\Theta = 7.5°$.

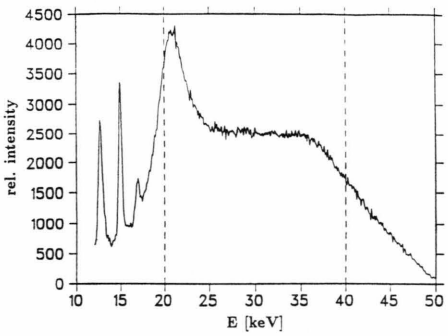

Fig. 4. Molten $Au_{28.5}Mn_{71.5}$; $T = 1145$ °C; $\Theta = 7.5°$; measured intensity.

4. Results and Discussion

4.1 Structure Factors

Figure 5 shows the total Faber-Ziman structure factor for the two Au_xMn_{1-x}-melts ($x = 68$; 28.5) in the Q-region up to 14 $Å^{-1}$ as obtained using the EDXD-method. We stress the point that both curves originally show oscillations for Q-values up to

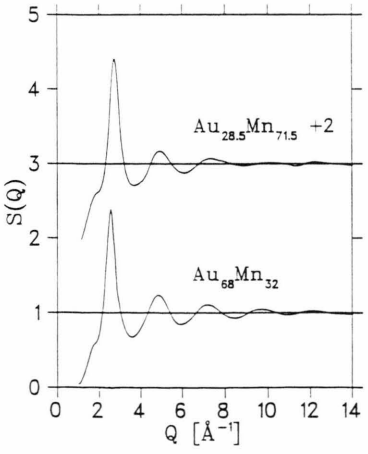

Fig. 5. Molten $Au_{28.5}Mn_{71.5}$ ($T = 1145$ °C); molten $Au_{68}Mn_{32}$ ($T = 1010$ °C); total Faber-Ziman structure factors $S(Q)$ according to the EDXD-method.

20 $Å^{-1}$, and that the pair correlation functions as obtained in Chapt. 4.2 were calculated using the full Q-range up to 20 $Å^{-1}$, which is important to obtain a good resolution in R-space.

For $Au_{28.5}Mn_{71.5}$ the main peak lies at 2.72 $Å^{-1}$ with a height of 2.41 and a width of 0.67 $Å^{-1}$. For $Au_{68}Mn_{32}$ the Q-value is smaller (2.55 $Å^{-1}$), but the height (2.39) and the width (0.65 $Å^{-1}$) are nearly the same.

For the second maximum the position (4.91 $Å^{-1}$ or 4.85 $Å^{-1}$), the height (1.17 or 1.24), as well as the width (1.04 $Å^{-1}$ or 1.06 $Å^{-1}$) for $Au_{28.5}Mn_{71.5}$ or $Au_{68}Mn_{32}$ are practically the same.

The shoulder at the left side of the main peak in each case indicates a premaximum at $Q=1.66$ $Å^{-1}$ or 1.64 $Å^{-1}$ for $x=28.5$ or 68, respectively.

The overall view shows that the upper curve (molten $Au_{28.5}Mn_{71.5}$) is more strongly damped than the lower curve, which may be explained by the higher melt-temperature of 1145 °C compared to 1010 °C. All data concerning the structure factors are compiled in Table 1.

Table 1. Molten $Au_{28.5}Mn_{71.5}$ (1145 °C) and $Au_{68}Mn_{32}$ (1010 °C). Structure factors; position, height, and full width at half maximum height (FWHM) of the peaks.

		$Au_{28.5}Mn_{71.5}$	$Au_{68}Mn_{32}$
Prepeak	position [$Å^{-1}$]	1.66	1.64
	height	0.58	0.55
	FWHM [$Å^{-1}$]	0.72	0.70
1st peak	position [$Å^{-1}$]	2.72	2.55
	height	2.41	2.39
	FWHM [$Å^{-1}$]	0.67	0.65
2nd peak	position [$Å^{-1}$]	4.91	4.85
	height	1.17	1.24
	FWHM [$Å^{-1}$]	1.04	1.06
3rd peak	position [$Å^{-1}$]	7.31	7.18
	height	1.07	1.11
	FWHM [$Å^{-1}$]	1.40	1.17

Table 2. Molten $Au_{28.5}Mn_{71.5}$ (1145 °C) and $Au_{68}Mn_{32}$ (1010 °C). Pair correlation functions; position R_i, FWHM ΔR_i, and coordination number Z_i.

	$Au_{28.5}Mn_{71.5}$	$Au_{68}Mn_{32}$
R_1 [Å]	2.79	2.82
ΔR_1 [Å]	0.67	0.58
Z_1	11.4	11.4
R_2^A [Å]	4.92	5.45
R_2^B [Å]	5.28	–
ΔR_2 [Å]	1.16	1.04
R_3 [Å]	7.40	8.13
ΔR_3 [Å]	1.23	1.13

4.2 Pair Correlation Functions

Figure 6 shows the pair correlation functions $G(R)$ as obtained from the Faber-Ziman structure factors by integration up to $Q_{max}=20$ $Å^{-1}$.

The dashed line at small R-values corresponds to $G(R)=-4\pi\varrho_0 R$.

In Table 2 the data as obtained from the pair correlation functions are compiled. For the $Au_{28.5}Mn_{71.5}$-melt the mean distance of nearest neighbours amounts to 2.79 Å, the width of the distribution to 0.67 Å, and the mean number of nearest neighbours to 11.4 atoms. For the $Au_{68}Mn_{32}$-melt the corresponding values are 2.82 Å, 0.58 Å, and 11.4 atoms. Also for the second and third maximum the width is larger for $x=28.5$ than for $x=68$. This effect can be explained by the higher temperature of 1145 °C in the first case compared to 1010 °C in the second. The positions of the maxima are always larger for the alloy with higher Au content ($x=68$), which is explained by the larger atomic diameter of the Au atoms.

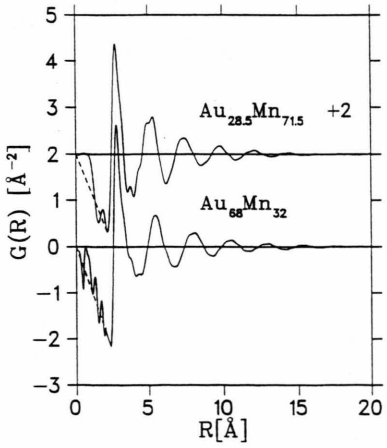

Fig. 6. Molten $Au_{28.5}Mn_{71.5}$ ($T=1145$ °C); molten $Au_{68}Mn_{32}$ ($T=1010$ °C); total Faber-Ziman pair correlation functions $G(R)$.

4.3 Chemical Short Range Order

For both melts, Fig. 7 shows the total Bhatia-Thornton structure factors. The dashed lines show the run to be expected without premaximum. Thus from

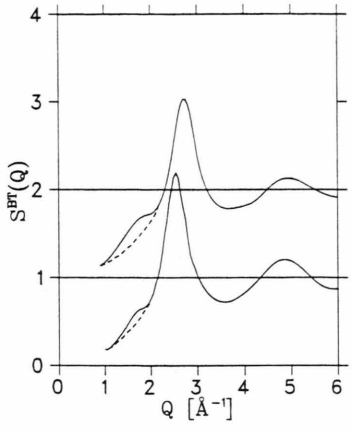

Fig. 7. Molten $Au_{28.5}Mn_{71.5}$ ($T=1145\,^{\circ}C$) (upper curve); molten $Au_{68}Mn_{32}$ ($T=1010\,^{\circ}C$) (lower curve); total Bhatia-Thornton structure factors $S^{BT}(Q)$ obtained using the EDXD-method.

the maximum difference between solid and dashed curves in both cases the position of the premaximum was determined. The chemical short range order causes a contribution to the total structure factor which corresponds to the Bhatia Thornton partial structure factor $S_{CC}(Q)$ which describes the correlation between concentration fluctuations. Usually the ratio of the position Q_P of the prepeak to the position Q_m of the main peak lies in the range $0.5 \leq Qp/Qm \leq 0.7$ with an ideal value of $Qp/Qm = 0.63$ [13]. The present results yield 0.64 for molten $Au_{68}Mn_{32}$ and 0.61 for molten $Au_{28.5}Mn_{71.5}$.

From the width ΔQ of the prepeak and of the main peak, respectively, the correlation length of the chemical short range order, ξ^C, and the correlation length of the topological short range order, ξ^T, can be estimated using the Scherrer equation [14] $\xi = 2\pi/\Delta Q$.

We obtain $\xi^C = 8.7$ Å or 9 Å for $x = 28.5$ or 68. The topological correlation length ξ^T shows the same tendency with the concentration: $\xi^T = 9.4$ Å or 9.7 Å for $x = 28.5$ or 68.

The maximum difference ΔS_P of the solid and the broken line at the prepeak in Fig. 7 is connected with $S_{CC}(Q_P)$, which is a measure for the chemical short range order via (7):

$$S_{CC}(Q_P) = \frac{\langle f^2 \rangle \Delta S_P}{(f_1 - f_2)^2 c_1 c_2}. \tag{7}$$

This allows to deduce from Fig. 7 the statement that the strength of the chemical short range order in the $Au_{68}Mn_{32}$-melt and in the $Au_{28.5}Mn_{71.5}$-melt are nearly the same but should be stronger in the first case according to thermodynamical measurements [6].

5. Conclusions

A Θ–Θ goniometer was supplied with a Si(Li)-detector in order to investigate molten Au_xMn_{1-x}-alloys ($x = 28.5$ and 68) with energy dispersive X-ray diffraction (EDXD). For the present alloys, the rather short measuring time proved to be very advantageous since by this choice the concentration variations caused by evaporation of Mn could be kept low.

Both melts show a prepeak which indicates compound formation in the melts. The chemical short range order is discussed by means of the total Bhatia-Thornton structure factors. The chemical short range order is the same in both melts. The total structure factors according to Faber-Ziman and the corresponding total pair correlation functions are presented together with the atomic distances and coordination numbers.

[1] B. Sedelmeyer, doctor thesis, University of Stuttgart (1985).
[2] B. C. Giessen and G. E. Gordon, Science **159,** 973 (1968).
[3] J. M. Prober and J. M. Schultz, J. Appl. Cryst. **8,** 405 (1975).
[4] T. Egami, J. Mat. Science **13,** 2587 (1978).
[5] R. Utz, A. Brunsch, P. Lamparter, and S. Steeb, Z. Naturforsch. **44a,** 1201 (1989).
[6] J. N. Pratt, J. Less-Comm. Met. **114,** 145 (1986).
[7] R. M. Hagenmayer, doctor thesis, University of Stuttgart (1992).
[8] T. E. Faber and J. M. Ziman, Phil. Mag. **11,** 153 (1965)
[9] R. Utz, doctor thesis, University of Stuttgart (1989).
[10] D. Lee, Ph. D. Thesis, University of California, Los Angeles (1980).
[11] H. F. Bühner, doctor thesis, University of Stuttgart (1970).
[12] K. Nishikawa, T. Jijima, Bull. Chem. Soc. Japan **57,** 1750 (1984).
[13] J. Blétry, Z. Naturforsch. **33a,** 327 (1977).
[14] P. Scherrer, Natur. Ges. Wiss. Göttingen, page 98 (1918).